Journal of Materials Chemistry A

Accepted Manuscript

ROYAL SOCIETY OF CHEMISTRY

www.rsc.org/materialsA

Journal of Materials Chemistry A RSCPublishing

ARTICLE

Surface modification of cobalt-free layered $Li[Li_{0.2}Fe_{0.1}Ni_{0.15}Mn_{0.55}]O_2$ oxide with $FePO_4/Li_3PO_4$ composite as the cathode for lithium-ion batteries

Cite this: DOI: 10.1039/xoxxoooooox

Received ooth January 2012,
Accepted ooth January 2012

DOI: 10.1039/xoxxoooooox

www.rsc.org/

Feng Wu[a,b], Xiaoxiao Zhang[a], Taolin Zhao[a], Li Li[a,b*], Man Xie[a] and Renjie Chen[a,b*]

Low-cost layered $Li[Li_{0.2}Fe_{0.1}Ni_{0.15}Mn_{0.55}]O_2$ is successfully coated with $FePO_4/Li_3PO_4$ composite by an aqueous solution method to achieve high electrochemical performances. X-ray diffraction (XRD) patterns indicate that modified sample is a hexagonal phase with minor crystalline Li_3PO_4 phase inside. Compared with pristine sample, modified ones show no change on morphology characterized by scanning electron microscope (SEM) analysis. However, an uniform coating layer of $FePO_4/Li_3PO_4$ composite can be observed clearly through transmission electron microscope (TEM) images. By electrochemical characterizations, the composite coating layer is proved to be beneficial for improving reversible capacity and cycling stability of modified sample (higher reversible discharge capacities of 192 mA h g^{-1} after 50 cycles with 3% coating amount). Surprisingly, high-rate capability is also exhibited to be improved with 3wt.% coating amount (125.3 mA h g^{-1} after 100 cycles at 10C). Furthermore, the voltage decay phenomenon during cycling is slowed down greatly and thus phase transformation is suppressed by the composite coating layer. These results are attributed to the suppression of bulk material from directly exposure with electrolyte by amorphous $FePO_4$ coating component and the good Li^+ transport through Li_3PO_4 coating component. The prepared modified materials can meet the requirement of low cost and high performances in various applications for lithium-ion batteries.

Introduction

To meet the energy storage requirements of various applications, such as portable devices, electric vehicles (EVs) and smart power stations,[1] low-cost cathode materials with high energy density should be developed for the next generation of lithium-ion batteries (LIBs). Considering the much higher capacity than the conventional $LiCoO_2$ cathode, Li-rich layered oxides are the most promising candidates to be qualified for those applications.[2–4] In these layered oxides, Fe-Mn based Li-rich cathodes without cobalt developed by Tabuchi et al,[5–10] such as $Li_{1+x}(Fe_{0.2}Ni_{0.2}Mn_{0.6})_{1-x}O_2$ and $Li_{1+x}(Fe_{0.2}Ni_{0.4}Mn_{0.4})_{1-x}O_2$, show their advantages in terms of high initial charge/discharge capacity and low cost. Although researchers all over the world have been investigating these materials with various compositions through different preparation methods, including sol-gel and coprecipitation, the poor cycling stability and rate capability are still the remaining drawbacks, which originate from the elimination of oxygen vacancies and phase transformation as well as the dissolution of transition metals, limiting their further development and application.[11–17]

Several strategies have been made to improve the electrochemical performances. For example, bulk substitution with metal or non-metal elements can stabilize the structure of electrode materials. In order to solve the poor rate capability, reducing the particle size to nanoscale is proved to be an effective method. Surface modification with a coating layer is another commonly used strategy to suppress the surface side reaction between the cathode material and electrolyte and reduce metal dissolution.[18, 19] Moreover, several coating materials have been proved to be able to retain oxygen vacancies and thus improve the discharge capacity.[20–23] Recently, it was reported that MPO_4 (M=Al, Fe, Ce et al.) phosphates are ideal coating material in terms of environmental friendliness, low cost and thermal stability.[24] In particular, $FePO_4$ coating was investigated to be very effective in retarding the oxygen loss.[25] There are some related reports about $FePO_4$ coated layered oxides cathodes ($LiCoO_2$, $LiCo_{1/3}Ni_{1/3}Mn_{1/3}O_2$) or other types of Li-rich cathodes[26-28] to improve their electrochemical performances. However, there are few reports to apply this promising coating material as a protective layer onto the surfaces of the low-cost cobalt-free Li-rich cathode.

Thus, we introduce $FePO_4$ coating layer onto the surface of cobalt-free Li-rich material $Li[Li_{0.2}Fe_{0.1}Ni_{0.15}Mn_{0.5}]O_2$ to achieve both low cost and high capacity as well as high rate capability. Moreover, the crystalline structure and morphology characterizations are discussed.

Experimental

The $Li[Li_{0.2}Fe_{0.1}Ni_{0.15}Mn_{0.5}]O_2$ powder was prepared by a coprecipitation process using hydroxide precursor. Nickel sulfate hexahydrate ($NiSO_4·6H_2O$), manganese sulfate monohydrate ($MnSO_4·H_2O$), iron sulfate heptahydrate ($FeSO_4·7H_2O$), sodium hydroxide (NaOH), and ammonium hydroxide ($NH_3·H_2O$) were used as starting reagents to prepare the precursor particles in a continuously stirred tank reactor (CSTR). During the coprecipitation reaction, 2 M transition metal solution (Fe:Ni:Mn=0.1:0.15:0.55) was slowly pumped into the reactor at 60 °C. The pH level was kept at 11 by controlling the added amount of the mixture solution of 4 M NaOH and 0.4 M $NH_3·H_2O$. The solution was strongly stirred at 1000 rpm. The reaction was conducted under an inert atmosphere by bubbling N_2 into the CSTR to mitigate the oxidation of Mn^{2+}, Ni^{2+} and Fe^{2+}. The spherical precursor was filtered, washed with deionized water and dried at 100 °C for 48 h in a vacuum oven. The dried precursor was well mixed with Li_2CO_3 and then calcined at 800 °C for 15 h to obtain the pristine cathode material $Li[Li_{0.2}Fe_{0.1}Ni_{0.15}Mn_{0.55}]O_2$, named as LLFNMO.

To coat the surface of $Li[Li_{0.2}Fe_{0.1}Ni_{0.15}Mn_{0.55}]O_2$ with $FePO_4$, a certain amounts of $Fe(NO_3)_3·9H_2O$ and $(NH_4)_2HPO_4$ were dissolved in deionized water, respectively. A desired amount of LLFNMO powder was dispersed in $(NH_4)_2HPO_4$ solution. The $Fe(NO_3)_3·9H_2O$ solution was then added into the mixture drop by drop for 3 h. Then, the resulting mixture was heated to 80 °C and stirred vigorously until the solution was evaporated to dryness. The obtained powder was heated at 400 °C in a muffle furnace for 5 h in air and then cooled to room temperature to get $FePO_4$-coated LLFNMO. Different coating amounts of 1 wt.%, 3 wt.% and 5 wt.% are named as FP-1, FP-3 and FP-5, respectively.

The structure analysis was carried out using X-ray diffraction (XRD; Rigaku Ultima IV-185) with a Cu Kα radiation source. The source tension and current are 40 kV and 40 mA, respectively. Data were acquired with a speed of 8° min^{-1} over a 2θ range of 10°−80°. Morphologies of the prepared samples were characterized by a field emission scanning electron microscope (FESEM, FEI, Quanta 200f) and transmission electron microscopy (TEM, JEM-2100f). Element mappings of the prepared samples were carried out with an energy dispersive X-ray detector (EDX). X-ray photoelectron spectroscopy (XPS, PHI Quantera) was used to detect the surface chemical state of the materials.

For fabrication of the cathodes, the prepared powders were mixed with acetylene black and polyvinylidene fluoride (8:1:1 by weight) in N-methyl-2-pyrrolidone (NMP). The obtained slurry was coated onto Al foil and roll-pressed. The electrodes were dried overnight at 80 °C in a vacuum oven. The electrode materials were assembled into 2025 coin-cells in a glove box filled with high-purity argon using Li metal as the anode for electrochemical measurements. The loading mass of active material in the samples is ~2.5 mg/cm^2. The electrolyte solution was 1 M $LiPF_6$ in ethyl carbonate (EC) and dimethyl carbonate (DMC) (1:1 by volume). The charge/discharge tests were performed using a Land battery test system (Land CT2001A, Wuhan, China) in the voltage range of 2.0−4.8 V at different current densities from 20 mA g^{-1} (0.1C) to 6000 mA g^{-1} (30C). A two-step charge process was employed at 0.1C and 0.2C. That is, the constant current charge step was followed by an additional constant voltage charge step until the current density dropped to half of its initial value. Electrochemical impedance spectroscopy (EIS) analysis was carried out from 10^5 Hz to 0.01 Hz using an IM6 electrochemical impedance analyzer with an AC perturbation signal of 5 mV. The potentials throughout the paper are referenced to the Li/Li^+ couple.

Results and discussion

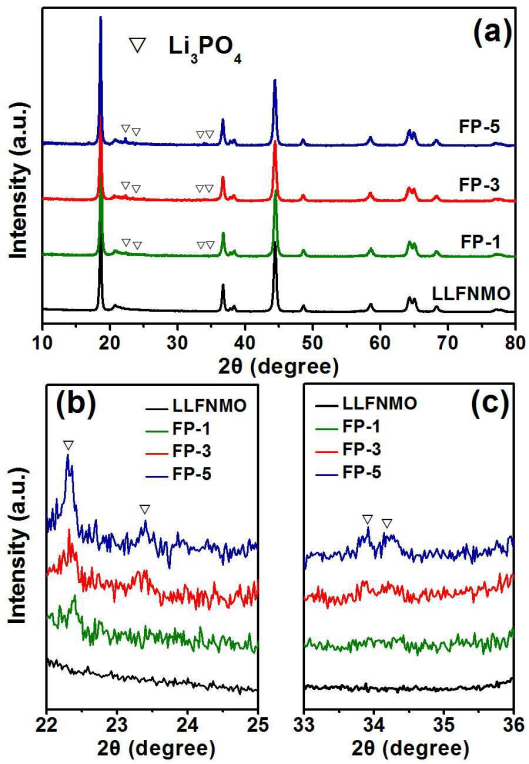

Fig. 1 XRD patterns of all the samples (a) and enlarged images in different 2θ degree (b, c).

Fig. 1a shows XRD patterns of LLFNMO and $FePO_4$-coated samples. LLFNMO exhibits patterns indexed to a hexagonal layered α-$NaFeO_2$ type structure (space group, $R\bar{3}m$) and some weak peaks in the range of 20–25° corresponding to the superlattice ordered $LiMn_6$ which exists in monoclinic Li_2MnO_3 phase (group symmetry, C2/m).[29, 30] In $FePO_4$-coated samples, there are no distinct diffraction peaks attributed to $FePO_4$ phase, due to its amorphous state. However, minor peaks of Li_3PO_4 phase formed by the out diffusion of lithium in the calcination process can be observed clearly in $FePO_4$-coated samples. The diffraction peaks of Li_3PO_4 phase increase with the increasing coating amounts, as shown in Fig. 1(b, c). Therefore, it is more reasonable to refer the $FePO_4$-coated sample as $FePO_4/Li_3PO_4$ composite coated sample. As a fast and stable Li ion conductor,[31] it is expected that Li_3PO_4 can increase the ionic transport at the surface of LLFNMO and

improve the rate capability. Fig. S1 shows the XRD patterns of the cycled electrodes of FP-3 after 100 cycles at 5C. It can be seen that after high rate cycling, all the diffraction patterns of FP-3 can still be indexed with a layered structure with no impurities. Meanwhile, the superlattice peaks between 20 and 23° have disappeared due to the transformation of Li_2MnO_3 component during cycling.

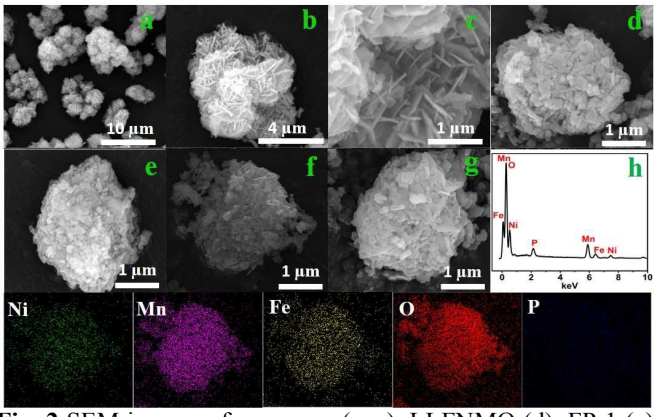

Fig. 2 SEM images of precursor (a–c), LLFNMO (d), FP-1 (e), FP-3 (f), FP-5 (g), EDS spectrum of FP-3 (h), and the elemental mapping distribution of Ni, Mn, Fe, O, P in FP-3.

SEM images of LLFNMO and $FePO_4/Li_3PO_4$-coated samples are depicted in Fig. 2. Coprecipitation method was employed to synthesize the spherical precursor with hierarchical structure, as shown in Fig. 2(a–c). The precursor particles are large agglomerates with 5~8 μm in diameter, and composed of secondary particles formed by polygonal nanoplates with a thickness of 50 nm. After calcination, LLFNMO is formed by nanoplates with a thickness of 100 nm (Fig. 2d). After modification with $FePO_4/Li_3PO_4$, great changes cannot be observed from SEM images (Fig. 2e, f, g). In addition, EDS was employed to verify the elements of FP-3 and the result is shown in Fig. 2h. It can be seen that FP-3 was indeed synthesized with expected elements, including Ni, Mn, Fe, O, and P. The uniform distribution of expected elements can also be clearly observed in the elemental mapping figure. SEM images of cycled FP-3 electrode after 100 cycles at 5C are shown in Fig. S2. The surface of materials become rough and some side reaction products are observed after cycling, while the whole structure of particles is maintained without obvious fracture.

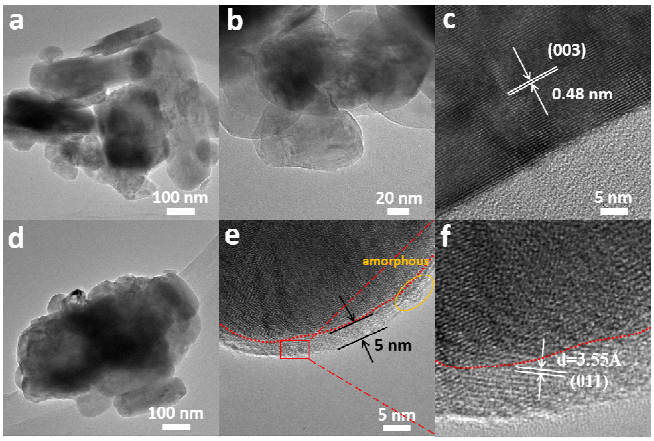

Fig. 3 TEM and HRTEM images of LLFNMO (a–c), and FP-3 (d–f).

Fig. 3 shows the TEM images of LLFNMO and FP-3 samples. The surface of LLFNMO is observed to be smooth and clean in Fig. 3(a, b) while FP-3 presents a rough surface in Fig. 3(d). High resolution TEM (HRTEM) images of LLFNMO and FP-3 are represented in Fig. 3(c, e and f). An interplanar spacing of layered LLFNMO was measured to be 0.48 nm, which is consistent with the other Li-rich materials without Fe element. After coating with $FePO_4/Li_3PO_4$, the bulk crystal lattice can be still retained. A coating layer can be clearly seen on the surface of the layered oxide with uniform distribution. The thickness is estimated to be 5 nm. In addition, the enlarged image of coating layer in Fig. 3f show that the coating layer was formed by two components, that is, the amorphous $FePO_4$ phase and the crystalline Li_3PO_4 phase. The distance of fringe in the coating layer is measured to be 3.55Å, which is the interplanar spacing of (011) planes in Li_3PO_4 phase and thus confirms the composition of the coating layer.This finding is consistent with the XRD results. Li_3PO_4 phase can accelerate the transportation of lithium ions. Together with the amorphous $FePO_4$ phase, the structure stability as well as electrochemical performances are speculated to be improved.

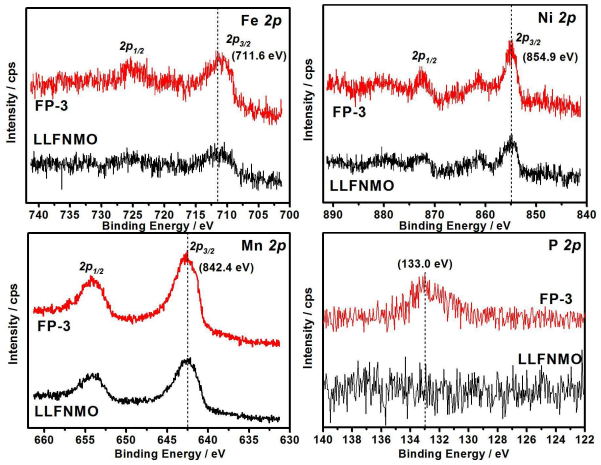

Fig. 4 XPS patterns of Fe, Ni, Mn, and P element in LLFNMO and FP-3 samples.

In order to investigate the changes of cathode surface property and the chemical states of Fe, Ni, Mn, and P elements in the surface coating layer, XPS was carried out on LLFNMO and FP-3, as shown in Fig. 4. The binding energy (BE) of Fe $2p_{3/2}$ is 711.6 eV, which is quite close to 711.2 eV of Fe^{3+}.[32] The Ni $2p_{3/2}$ XPS spectra have a BE of 854.9 eV, in accordance with Ni^{2+} in $Li[Li_{1/3-2x/3}Ni_xMn_{2/3-x/3}]O_2$ compounds.[33] The Mn $2p_{3/2}$ peak fits well with a BE of 642.4 eV, which is in a good agreement with the typical value of Mn^{4+} oxidation state (642.4 eV) in manganese-based layered compounds.[34] So it can be concluded that the Fe, Ni, Mn ions exist mainly in the form of Fe^{3+}, Ni^{2+}, Mn^{4+} in LLFNMO and FP-3. Besides, the binding energy of P 2p in FP-3 is around 133.0 eV, which is consistent with the value reported for P^{5+} in PO_4^{3-},[35, 36] while the P 2p peaks in LLFNMO cannot be detected as expected. Thus, it comes to the conclusion that the material coated on the surface of LLFNMO presents in the form of $FePO_4$ and Li_3PO_4.

The first charge/discharge profiles and the corresponding differential capacity vs. voltage profiles of LLFNMO and $FePO_4/Li_3PO_4$-coated samples at 0.2C between 2.0 and 4.8 V are shown in Fig. 5, which can evaluate the effects of $FePO_4/Li_3PO_4$ coating layer on the electrochemical properties

of LLFNMO. Two plateaus can be observed in the first charge profile for all the samples. The first plateau region below 4.5 V is formed by the lithium extraction from the layered component, belonging to the oxidation of Ni^{2+} and Fe^{3+}. The second long plateau region around 4.5 V is attributed to the simultaneous extraction of lithium ion and oxygen from Li_2MnO_3 lattice.[37,38] The oxidation process at 4.5 V is irreversible which can be verified by the trend of discharge profiles and the absence of reduction peaks at 4.5 V. The appearance of reduction peaks at 3.3 V result from the reduction of Mn^{4+} to Mn^{3+}, which is activated after charging above 4.5 V during the first charge process.

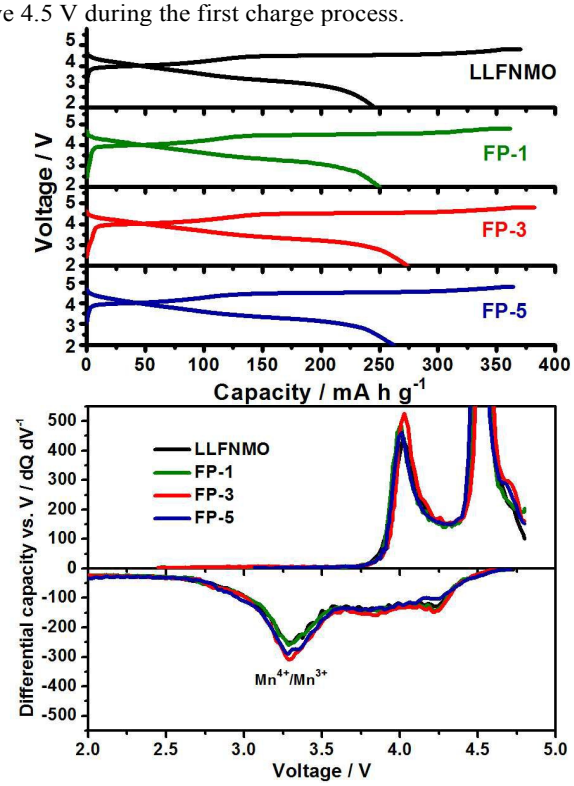

Fig. 5 First charge/discharge profiles at 0.2C between 2 and 4.8 V, and the corresponding differential capacity vs. voltage curves.

Fig. 6 compares the changes of several electrochemical parameters at the first cycle in the samples before and after coating, including charge capacity, discharge capacity, Coulombic efficiency and medium discharge voltage. As it can be seen, FP-3 delivers higher first charge capacity of 382.4 mA h g^{-1} than that of LLFNMO (370.5 mA h g^{-1}). The first discharge capacity presents an upward trend with the increasing coating amount until that FP-3 achieves the highest initial discharge capacity of 273.9 mA h g^{-1}, which is much higher than 246.2 mA h g^{-1} of LLFNMO. However, when the coating amount increases to 5 wt.%, the discharge capacity of FP-5 was decreased to 262.2 mA h g^{-1}, probably due to the difficulty of charge transfer through a thicker coating layer and the electrochemical inactive characteristic of amorphous $FePO_4$. In addition, the Coulombic efficiency of the first cycle increases with the increasing coating amount but much improvement cannot be achieved by coating more amount of $FePO_4/Li_3PO_4$ according to the trend. The highest Coulombic efficiency reaches to be 72% in FP-5. The medium discharge voltage rises first when the coating amount is lower than 5 wt.% and reaches to its highest data of 3.455 V obtained by FP-3, then decreases when coating more amount of $FePO_4/Li_3PO_4$. In short, the improvements of initial charge/discharge capacities, Coulombic efficiency and medium discharge voltage can be attributed to that the amorphous $FePO_4$ can prevent the bulk material from the direct exposure to the electrolyte and thus the suppression of surface side reaction. Meantime, the crystalline Li_3PO_4 phase can accelerate Li^+ transportation effectively during charge and discharge processes.[28]

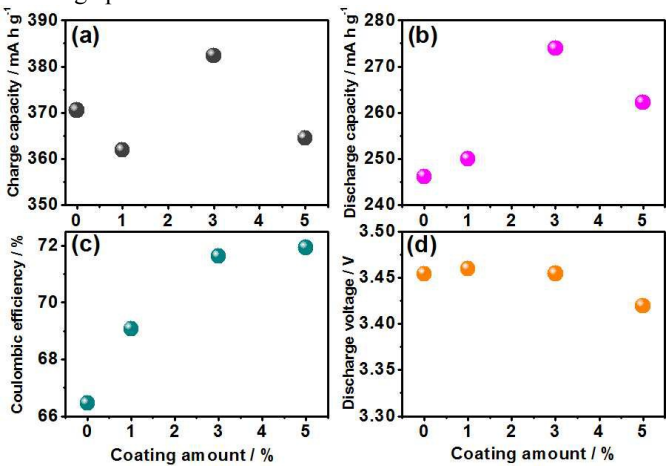

Fig. 6 Changes of several parameters of all the samples at the first cycle: initial charge and discharge capacities (a, b), Coulombic efficiencies (c) and medium discharge voltage (d).

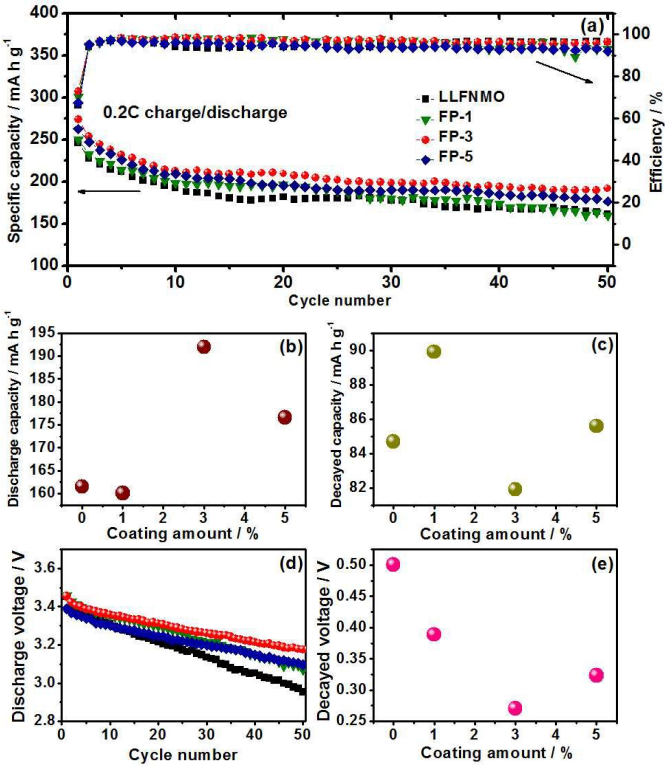

Fig. 7 Cycling performances of all the samples at 0.2C (a), discharge capacity and capacity loss after 50 cycles (b, c), medium discharge voltage (d), and decayed voltage (e).

Cycling stabilities and Coulombic efficiencies of all the samples at 0.2C are depicted in Fig. 7. It can be clearly seen that FP-3 delivers higher reversible discharge capacities of 192 mA h g^{-1} after 50 cycles than that of pristine LLFNMO (161.5

mA h g^{-1}). And the Coulombic efficiencies of FP-3 are also higher and more stable than the other samples. Capacity retentions of LLFNMO and FP-3 are 65.6% and 70.1%, respectively. That is, the decayed discharge capacity of FP-3 is obviously lower than that of the pristine one, as depicted in Fig. 7c. In addition, the medium discharge voltages during cycling decrease for all the samples, which is the drawback of Li-rich layered oxides due to the phase transformation from layered to spinel. Notably, the medium discharge voltage of FP-3 is always higher than the other samples during cycling (Fig. 7d). That is, the decayed voltage of FP-3 after 50 cycles shows the smallest value of 0.27 V compared with that of the pristine one (0.5 V), as shown in Fig. 7e.

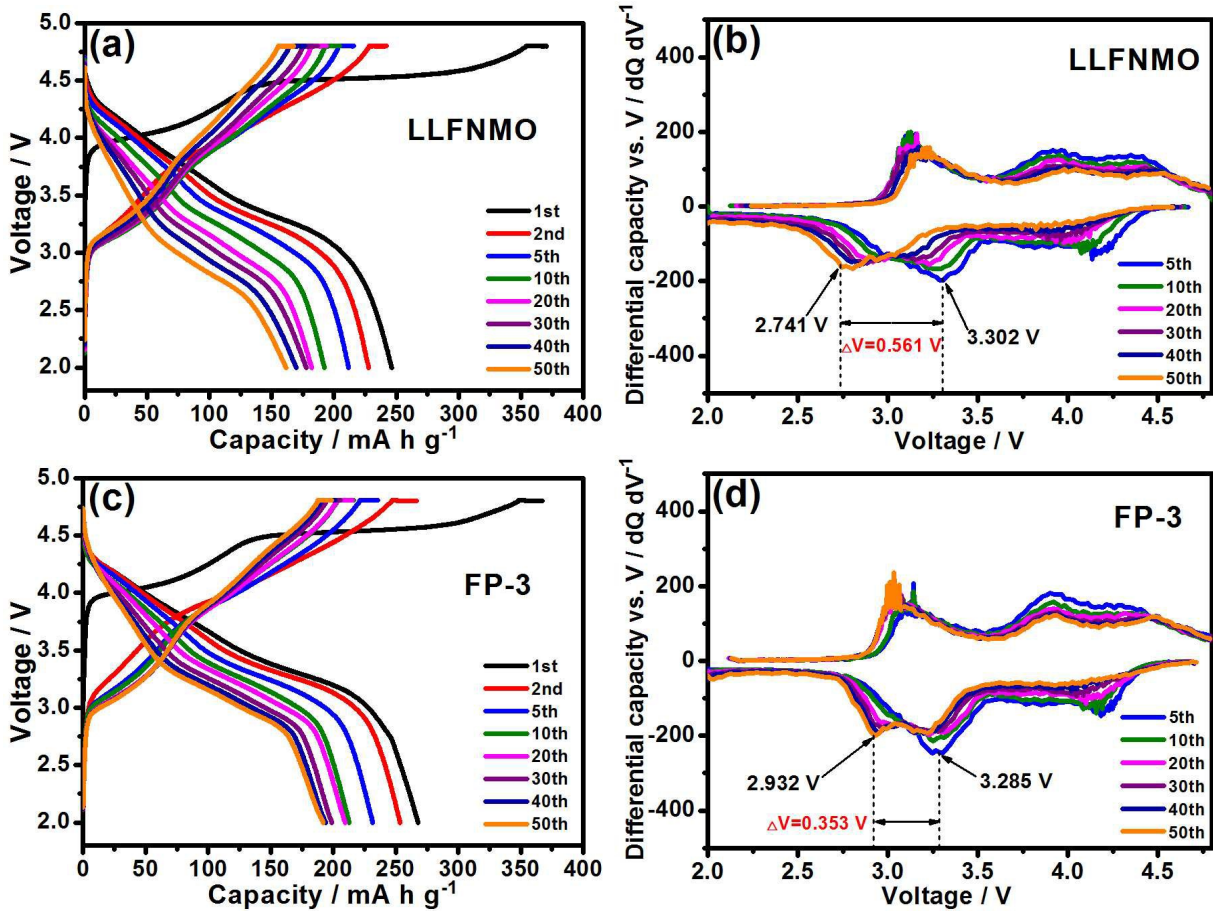

Fig. 8 Charge/discharge profiles at different cycles at 0.2C and the corresponding differential capacities curves of LLFNMO (a, b) and FP-3(c, d).

In order to further investigate the suppression of voltage decay in coated samples, the charge/discharge profiles of different cycles and the corresponding differential capacity curves of LLFNMO and FP-3 samples are shown in Fig. 8. The decayed discharge voltages of all the samples are mainly originated from the decayed voltage at 3.3 V, in which process the structure was transformed from the layered to spinel during cycling. Different from the term of medium discharge voltage to illustrate the voltage decay phenomenon, here we use the shift of discharge voltage peak position (Δ V) at 3.3 V to demonstrate the suppression of voltage decay with coated sample, which can be clearly observed in differential capacity curves.[39] The decayed discharge voltage after 50 cycles at 0.2C at 3.3 V is reduced from 0.561 V to 0.353 V by coating 3wt.% $FePO_4/Li_3PO_4$. Moreover, the reduction peak of $Mn^{4+/3+}$ at 3.3 V still exists for the coated sample after 50 cycles, meaning the remaining of layered structure. By comparison, the layered structure of $LiMnO_2$ in LLFNMO is transformed completely to the spinel phase, as can be seen from the disappearance of the reduction peak of $Mn^{4+/3+}$ at 3.3 V after 50 cycles. From these results, it is reasonable to conclude that the $FePO_4/Li_3PO_4$ coating layer can suppress the capacity fading and discharge voltage decay during charge/discharge cycles, that is, the suppression of transformation from layered to spinel phase.

The differential capacity vs. voltage at the same cycle number at 0.2C of all the samples are compared in Fig. S3 to investigate the effect of coating amount on the suppression of decayed voltage. There are great changes in the oxidation (orange rectangle) and reduction (pink rectangle) reaction positions with cycling. The peak positions of the rectangles at 5th cycle of $FePO_4/Li_3PO_4$ coated samples are almost the same with LLFNMO. During cycling, the oxidation and reduction peaks shift left gradually due to the structure transformation from layered to spinel. Meanwhile, the peak separation between LLFNMO and $FePO_4/Li_3PO_4$ coated samples become gradually obvious during cycling. The reduction peak positions of $FePO_4/Li_3PO_4$ coated samples are always higher than those of pristine ones. FP-1 and FP-5 have a similar trend of discharge voltage shift, and FP-3 still shows apparent reduction peak of layered $Mn^{4+/3+}$ at 3.3 V at the 50th cycle compared with LLFNMO. These results indicate that less spinel is formed

during cycling for the $FePO_4/Li_3PO_4$ coated sample than those of LLFNMO. The coating amount should be adjusted to obtain the optimal electrochemical performances, and FP-3 with 3wt.% coating amount exhibits the best structure stability among all the samples.

Fig. S4a and S4b show the electrochemical performances of all the samples at 0.5C and 1C, respectively. All the electrodes are cycled at 0.1C in the first three cycles to activate the Li_2MnO_3 component. Obviously, both the reversible discharge capacities and cycling stabilities are improved by the introduction of $FePO_4/Li_3PO_4$ coating layer. Except the large irreversible capacity loss at the first cycle, the following Coulombic efficiencies of all the samples are close to 99%. After 100 cycles, FP-3 delivers the highest reversible discharge capacities of 167 mA h g^{-1} at 0.5C and 166.5 mA h g^{-1} at 1C, much higher than those of LLFNMO (115.8 mA h g^{-1} at 0.5C and 106 mA h g^{-1} at 1C). Based on the discharge capacities of 4th cycle, capacity retentions of FP-3 at 0.5C and 1C are 77.9% and 90.7%, respectively, which are also much higher than those of LLFNMO (63.8% and 61.7%). From the charge/discharge profiles at different cycles and the corresponding differential capacity curves at 0.5C and 1C (Fig. S4c–f), the decayed discharge voltages at 3.3 V of FP-3 are lower than those of LLFNMO sample. At 0.5C cycling rate, the decayed discharge voltage at 3.3 V after 50 cycles is reduced from 0.602 V to 0.357 V by coating 3wt.% $FePO_4/Li_3PO_4$. As for 1C rate, the reduced voltage decay at 3.3 V is also obviously observed from 0.545 V to 0.355 V.

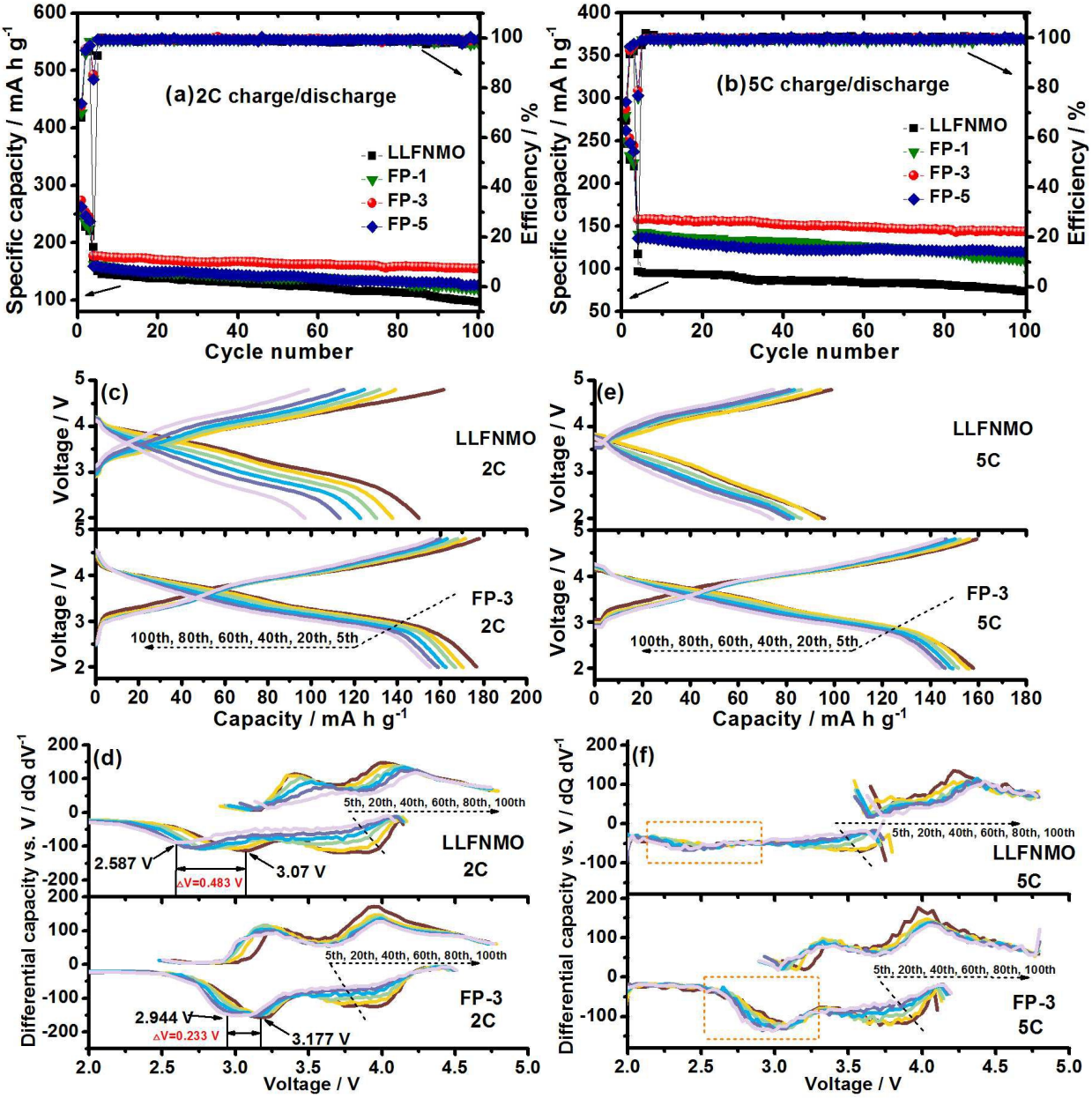

Fig. 9 Cycling performances of all the samples at 2C (a) and 5C (b), the charge/discharge profiles of different cycles and the corresponding differential capacities curves of LLFNMO and FP-3 at 2C (c and d) and 5C (e and f).

Cycling performances and Coulombic efficiencies of LLFNMO and FP-3 at 2C and 5C are depicted in Fig. 9. Obviously, FP-3 delivers higher reversible discharge capacities after 100 cycles, 155.3 mA h g^{-1} at 2C and 143.8 mA h g^{-1} at 5C than those of

LLFNMO (97.2 mA h g^{-1} at 2C and 74.2 mA h g^{-1} at 5C). Based on the discharge capacities of 4th cycle, capacity retentions of FP-3 at 2C and 5C are 87.6% and 90.9% respectively, which are also much higher than those of LLFNMO (58.1% and 63.3%). Notably, the decayed discharge voltages of FP-3 are also lower than those of LLFNMO sample, which can be seen from the charge/discharge profiles at different cycles and the corresponding differential capacity curves. When cycling at 2C, the decayed discharge voltage at 3.3 V is reduced from 0.483 V to 0.233 V after coated with 3wt.% $FePO_4/Li_3PO_4$. As for 5C high rate, there is no obvious shift of reduction peak during cycling for both samples. While the reduction peak of FP-3 is located at much positive position (about 3 V) than that of LLFNMO (2.5 V). From these results, it is reasonable to conclude that the capacity fading and discharge voltage decay during charge/discharge cycles are effectively suppressed by the introduction of $FePO_4/Li_3PO_4$ coating layer even at higher cycling rates.

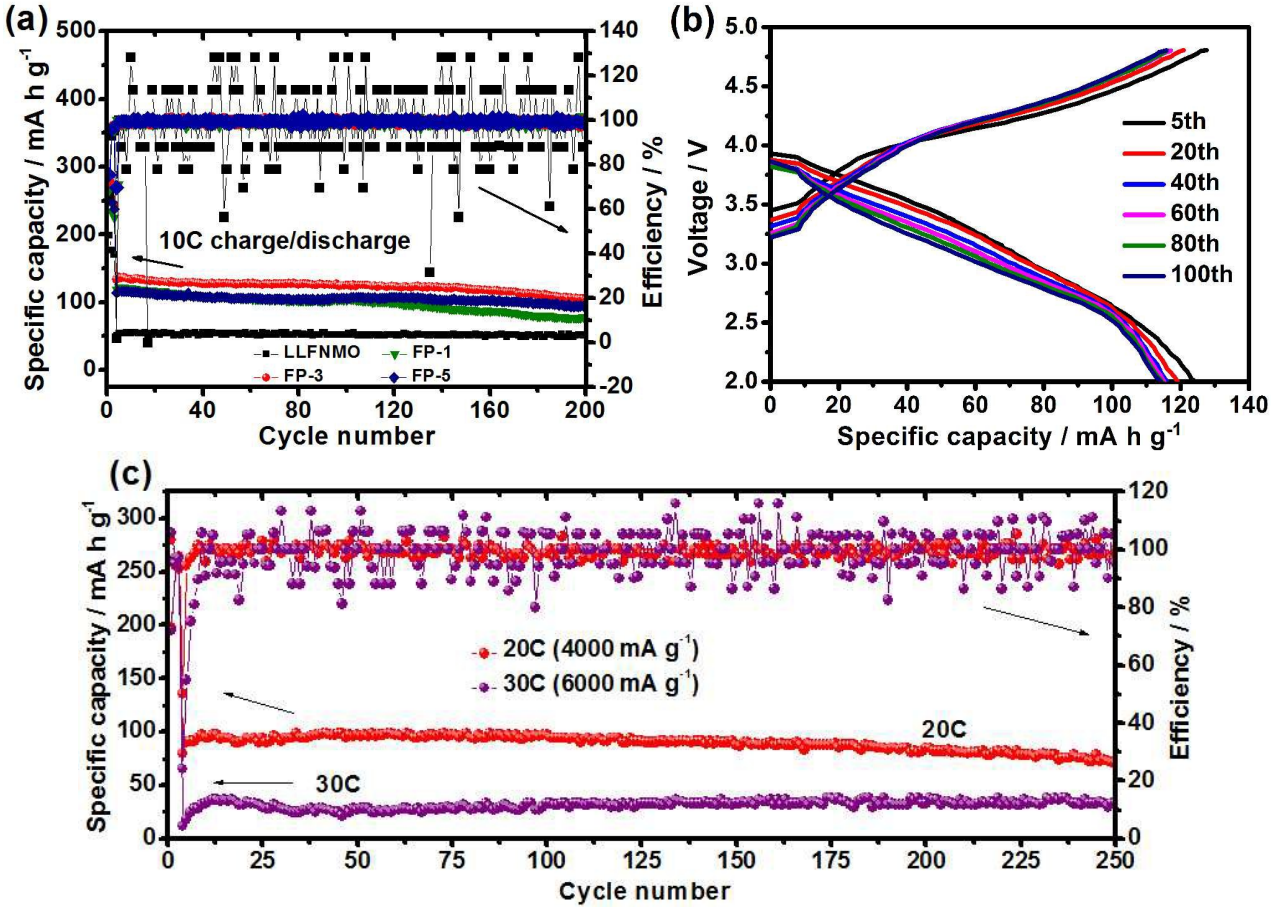

Fig. 10 Cycling performances of all the samples at 10C (a), the charge/discharge profiles of different cycles of FP-3 at 10C (b), cycling performances at 20C and 30C of FP-3 (c).

Cycling performances and Coulombic efficiencies of all the samples at 10C are shown in Fig. 10. Obviously, the high-rate capability can be much improved by $FePO_4/Li_3PO_4$ coating layer. When the coating amount is 3wt.%, the highest reversible capacity of 125.3 mA h g^{-1} at 100th cycle and 103.4 mA h g^{-1} at 200th cycle can be delivered, which is much higher than that of LLFNMO sample. In addition, the Coulombic efficiencies of $FePO_4/Li_3PO_4$ coated samples are all more stable than that of LLFNMO sample (Fig. 10a). The charge/discharge curves of FP-3 at 10C are shown in Fig. 10b. Good reversibility can be concluded from the almost overlaps of charge/discharge curves. To further demonstrate the excellent high-rate capability of FP-3 sample, 250 cycles was tested at 20C and 30C and the results are shown in Fig. 10c. Even cycled at the ultra-high rates, good cycling stability and high reversible discharge capacity can also be obtained. The reversible discharge capacity after 250 cycles are 71.5 mA h g^{-1} at 20C and 34 mA h g^{-1} at 30C, respectively. The excellent rate capability can be considered to result from the reduction of the contact between bulk material and electrolyte as well as the positive role of Li_3PO_4 component.

Fig. 11 shows the EIS profiles of the electrodes at open circuit potential. The impedance spectrum is composed of a high-frequency semicircle and a low-frequency slope, as in standard Nyquist plots. The diameter of the semicircle represents the charge-transfer resistance (R_{ct}). The intercept of the semicircle with the horizontal axis (Z') at the high frequency refers to the uncompensated ohmic resistance of the electrolyte (R_Ω) and the rising line in low-frequency section is related to the Warburg impedance (Z_W), which is associated with the diffusion of Li^+ into the bulk material.[40] The ohmic resistance (R_Ω) and "faradaic impedance" (the combination of R_{ct} and Z_W) reflect the kinetics of the cell reactions.[29] Obviously, the R_{ct} value of FP-3 is about 50 Ω, which was smaller than that of LLFNMO (90 Ω), indicating the better reaction kinetics and thus the improved electrochemical performances. The diffusion coefficient, D_{Li+}, can be calculated in terms of the following equation:[41]

$$D_{Li^+} = \frac{R^2T^2}{2\sigma^2A^2C^2F^4n^4} \qquad (1)$$

where R is the gas constant, T is the absolute temperature, n is the number of transferred electrons, F is the Faraday constant, A is the surface area of the electrode, C is the concentration of Li^+ in the electrode, and σ is Warburg factor obeying the relationship:

$$Z_{re} = \sigma \cdot \varpi^{-1/2} \quad (2)$$

The lithium diffusion coefficient D_{Li+} of FP-3 are calculated to be 1.003×10^{-17} cm^2 s^{-1}, which is higher than that of LLFNMO (3.389×10^{-18} cm^2 s^{-1}), demonstrating the better lithium intercalation kinetics in the coated electrode. Moreover, the Nyquist impedance plot of FP-3 exhibits a line with a bigger slope in the low frequency region, indicating a characteristic of capacitive property. Besides, the impedances of the cells at charged state of 4 V are compared after 100 cycles at 5C. The results in Fig. S5 show that the semicircle in the low frequency of FP-3 is obviously smaller than that of LLFNMO, which stands for the smaller Rct. Thus, it is reasonable to exhibit the high rate performance in the coated electrodes.

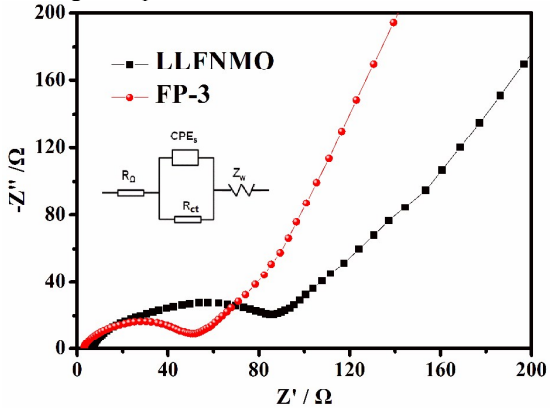

Fig. 11 The Nyquist plots of the LLFNMO and FP-3 before cycling.

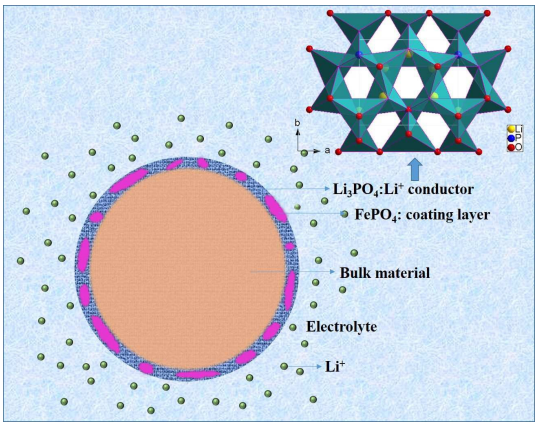

Fig. 12 A schematic representation of $FePO_4/Li_3PO_4$ composite coating layer.

According to above results, the improvement in the electrochemical performances of FP-3 can be ascribed to the introduction of the coating layer. The composite coating layer composed of amorphous $FePO_4$ and crystalline Li_3PO_4, which is different from the single and double coating layers, is evenly distributed in the surface of bulk materials, as shown in Fig. 12. Firstly, the amorphous $FePO_4$ coating layer can reduce the contact with electrolyte, thus suppressing the side reaction. Secondly, the Li_3PO_4 phase on the surface can act as Li^+ conductor, which is beneficial to the rate performances. Moreover, the composite coating layer can suppress the layered to spinel phase transformation during cycling. Although the exact mechanism of the stabilization of the structure by the coating layer is not clear, it is speculated that the coating layer may relieve the formation of spinel in the $R\bar{3}m$ phase.[42]

Conclusions

In summary, a composite coating layer containing amorphous $FePO_4$ and crystalline Li_3PO_4 was successfully coated onto the surface of $Li[Li_{0.2}Fe_{0.1}Ni_{0.15}Mn_{0.5}]O_2$ cathode material via a wet chemical method. Compared with the pristine sample, the surface modified samples showed the crystalline Li_3PO_4 phase in XRD patterns. A uniform nano coating layer (~5 nm) can be observed clearly in modified sample from TEM images. The results of electrochemical characterizations reveal that the composite coating layer plays a pivotal role as protective layer to suppress the capacity fading and discharge voltage decay during charge/discharge cycles and improve rate capability. EIS analysis shows that the charge transfer resistance of surface modified sample is lower than that of pristine one, indicating better rate performance of coated sample. In addition, the effects of Li_3PO_4 phase as a Li^+ conductor cannot be neglected. It demonstrates the significance of stable $FePO_4$ coating on low-cost Li-rich electrode materials to achieve both low cost and high performances for LIBs.

Acknowledgements

The experimental work of this study was supported by the Chinese National 973 Program (2015CB251100), the National Science Foundation of China (NSFC 51302014), Beijing Nova Program (Z121103002512029) and the New Century Educational Talents Plan of the Chinese Education Ministry (NCET-12-0050).

Notes

[a] Beijing Key Laboratory of Environmental Science and Engineering, School of Chemical Engineering and the Environment, Beijing Institute of Technology, Beijing 100081, P. R.China.
[b] National Development Center for High Technology Green Materials, Beijing 100081, P. R.China.
Corresponding author: E-mail address: lily863@bit.edu.cn

References

1 S. B. Chikkannanavar, D. M. Bernardi and L. Liu, *J. Power Sources*, 2014, **248**, 91.
2 J. Hong, D.-H. Seo, S.-W. Kim, H. Gwon, S.-T. Oh and K. Kang, *J. Mater. Chem.*, 2010, **20**, 10179.
3 T. Zhao, S. Chen, L. Li, X. Zhang, R. Chen, I. Belharouak, F. Wu and K. Amine, *J. Power Sources*, 2013, **228**, 206.
4 Z. Lu, L. Y. Beaulieu, R. A. Donaberger, C. L. Thomas and J. R. Dahn, *J. Electrochem. Soc.*, 2002, **149**, A778.
5 M. Tabuchi, A. Nakashima, H. Shigemura, K. Ado, H. Kobayashi, H. Sakaebe, H. Kageyama, T. Nakamura, M. Kohzaki, A. Hirano and R. Kanno, *J. Electrochem. Soc.*, 2002, **149**, A509.
6 M. Tabuchi, Y. Nabeshima, K. Ado, M. Shikano, H. Kageyama and K. Tatsumi, *J. Power Sources*, 2007, **174**, 554.
7 J. Kikkawa, T. Akita, M. Tabuchi, M. Shikano, K. Tatsumi and M. Kohyama, *J. Electrochem. Soc.*, 2009, **156**, A839.

8 M. Tabuchi, Y. Nabeshima, T. Takeuchi, K. Tatsumi, J. Imaizumi and Y. Nitta, *J. Power Sources*, 2010, **195**, 834.
9 J. Kikkawa, T. Akita, M. Tabuchi, K. Tatsumi and M. Kohyama, *J. Electrochem. Soc.*, 2011, **158**, A760.
10 K. Nakahara, M. Tabuchi, S. Kuroshima, A. Toda, K. Tanimoto and K. Nakano, *J. Electrochem. Soc.*, 2012, **159**, A1398.
11 M. Tabuchi, Y. Nabeshima, T. Takeuchi, H. Kageyama, K. Tatsumi, J. Akimoto, H. Shibuya and J. Imaizumi, *J. Power Sources*, 2011, **196**, 3611.
12 M. Tabuchi, Y. Nabeshima, T. Takeuchi, H. Kageyama, J. Imaizumi, H. Shibuya and J. Akimoto, *J. Power Sources*, 2013, **221**, 427.
13 K. Karthikeyan, S. Amaresh, G. W. Lee, V. Aravindan, H. Kim, K. S. Kang, W. S. Kim and Y. S. Lee, *Electrochim. Acta*, 2012, **68**, 246.
14 D. Uzun, M. Doğrusöz, M. Mazman, E. Biçer, E. Avci, T. Şener, T. C. Kaypmaz and R. Demir-Cakan, *Solid State Ionics*, 2013, **249-250**, 171.
15 T. Zhao, L. Li, S. Chen, R. Chen, X. Zhang, J. Lu, F. Wu and K. Amine, *J. Power Sources*, 2014, **245**, 898.
16 K. Karthikeyan, S. Amaresh, S. H. Kim, V. Aravindan and Y. S. Lee, *Electrochim. Acta*, 2013, **108**, 749.
17 J. Li, L. Wang, L. Wang, J. Luo, J. Gao, J. Li, J. Wang, X. He, G. Tian and S. Fan, *J. Power Sources*, 2013, **244**, 652.
18 Z. Chen, Y. Qin, K. Amine and Y. K. Sun, *J. Mater. Chem.*, 2010, **20**, 7606.
19 X. Wu, X. Li, Z. Wang, H. Guo, P. Yue and Y. Zhang, *Appl. Surf. Sci.*, 2013, **268**, 349.
20 J. M. Zheng, J. Li, Z. R. Zhang, X. J. Guo and Y. Yang, *Solid State Ionics*, 2008, **179**, 1794.
21 J. Gao, J. Kim and A. Manthiram, *Electrochem. Commun.*, 2009, **11**, 84.
22 Y. Wu and A. Manthiram, *Solid State Ionics*, 2009, **180**, 50.
23 X. Xiong, Z. Wang, G. Yan, H. Guo and X. Li, *J. Power Sources*, 2014, **245**, 183.
24 Y. Bai, X. Wang, S. Yang, X. Zhang, X. Yang, H. Shu and Q. Wu, *J. Alloys Compd.*, 2012, **541**, 125.
25 H. Lee, Y. Kim, Y.-S. Hong, Y. Kim, M. G. Kim, N.-S. Shin and J. Cho, *J. Electrochem. Soc.*, 2006, **153**, A781.
26 G. Li, Z. Yang and W. Yang, *J. Power Sources*, 2008, **183**, 741.
27 X. Liu, H. Li, E. Yoo, M. Ishida and H. Zhou, *Electrochim. Acta*, 2012, **83**, 253.
28 Z. Wang, E. Liu, C. He, C. Shi, J. Li and N. Zhao, *J. Power Sources*, 2013, **236**, 25.
29 A. R. Armstrong, M. Holzapfel, P. Novák, C. S. Johnson, S.-H. Kang, M. M. Thackeray and P. G. Bruce, *J. Am. Chem. Soc.*, 2006, **128**, 8694.
30 M. M. Thackeray, S.-H. Kang, C. S. Johnson, J. T. Vaughey, R. Benedek and S. A. Hackney, *J. Mater. Chem.*, 2007, **17**, 3112.
31 G. Tan, F. Wu, L. Li, R. Chen and S. Chen, *J. Phys. Chem. C*, 2013, **117**, 6013.
32 T. Yamashita and P. Hayes, *Appl. Surf. Sci.*, 2008, **254**, 2441.
33 N. Tran, L. Croguennec, C. Labrugère, C. Jordy, P. Biensan and C. Delmas, *J. Electrochem. Soc.*, 2006, **153**, A261.
34 K. M. Shaju, G. V. Subba Rao and B. V. R. Chowdari, *Electrochim. Acta*, 2002, **48**, 145.
35 Q. Y. Wang, J. Liu, A. V. Murugan and A. Manthiram, *J. Mater. Chem.*, 2009, **19**, 4965.
36 Y. Wu, A. Vadivel Murugan and A. Manthiram, *J. Electrochem. Soc.*, 2008, **155**, A635.
37 Y. Wu and A. Manthiram, *J. Power Sources*, 2008, **183**, 749.
38 N. Yabuuchi, K. Yoshii, S. T. Myung, I. Nakai and S. Komaba, *J. Am. Chem. Soc.*, 2011, **133**, 4404.
39 F. Wu, Z. Wang, Y. Su, Y. Guan, Y. Jin, N. Yan, J. Tian, L. Bao and S. Chen, *J. Power Sources*, 2014, **267**, 337.
40 K. Tan, M. Reddy, G. Rao and B. Chowdari, *J. Power Sources*, 2005, **141**, 129.41 Z. Li, Y. Wang, X. Bie, K. Zhu, C. Wang, G. Chen and Y. Wei, *Electrochem. Commun.*, 2011, **13**, 1016.
41 Z. Li, Y. Wang, X. Bie, K. Zhu, C. Wang, G. Chen and Y. Wei, *Electrochem. Commun.*, 2011, **13**, 1016.
42 M. Gu, I. Belharouak, J. M. Zheng, H. M. Wu, J. Xiao, A. Genc, K. Amine, S. Thevuthasan, D. R. Baer, J. G. Zhang, N. D. Browning, J. Liu and C. M. Wang, *ACS Nano*, 2013, **7**, 760.